Multi-Meson Model applied to $D^+ \to K^+K^-K^+$

R. T. Aoude[a], P. C. Magalhães[a], A. C. dos Reis[a] and M. R. Robilotta[b]

[a] *Centro Brasileiro de Pesquisas Físicas – CBPF, Rio de Janeiro, RJ, Brazil*

[b] *Instituto de Física, Universidade de São Paulo, São Paulo, SP, Brazil*[*]

(Dated: April 12, 2016)

arXiv:1604.02904v1 [hep-ph] 11 Apr 2016

Abstract

Matrix elements of weak currents involving light multi-meson states are important in many hadronic decays of both heavy leptons and heavy mesons. In this paper we focus on the latter case where the current size of the data set demands better models. The specific case of three-kaon weak matrix elements is considered and expressed as a relatively simple structure, which generalizes naturally the concept of form factor. We propose a model for the decay $D^+ \to K^+K^-K^+$ as an alternative to isobar model, with free parameter predicted by the theory to be fine-tuned by a fit to data. An important qualitative outcome is that we encompass naturally all final states topologies, which involve necessarily proper multi-particle structures and cannot be decomposed into simpler two-body processes. This aspect represents a significant improvement when compared to isobar model, often employed in analyses of heavy-meson decay data.

[*] pmagalhaes@cbpf.br

I. INTRODUCTION

Three-body, nonleptonic decays of heavy-flavoured mesons are sequential processes, dominated by intermediate resonant states. For this reason, these decays have been extensively used to study light meson spectroscopy. For the same reason, these decays have been also used for direct CP violation searches. The phase variation of the resonances provides the strong phase difference required for CP violation to occur.

The determination of the resonant structure of three-body decays requires a full amplitude analysis. The key issue in such analysis is the modelling of the decay amplitude. The usual experimental approach is to represent the decay amplitude as a coherent sum of resonant amplitudes, $\mathcal{A} = \sum c_k A_k$. The relative contribution of the different resonant amplitudes are derived from the complex coefficients c_k, which are the usual fit parameters. This is known as the isobar model.

The isobar model provides an effective description of the Dalitz plot of many different final states, for data sets up to $\mathcal{O}(10^4)$ events [1]. However, the analysis of the gigantic samples of B and D decays collected by the LHC experiments demands better models.

A particularly important issue is the representation of the nonresonant component of the decay amplitude. In general, the nonresonant amplitude used to fit data is parametrized by ad hoc functions that are not compromised with any theory. This component is typically small in D meson decays, and it is usually assumed to be constant across the Dalitz plot [1]. In B decays, however, where the contribution of the nonresonant component may be large, empirical formulas have been used to fit the data. These formulas may provide an effective representation of the available data, but the lack of theoretical justification and the interplay between the nonresonant amplitude and the broad scalar resonances at low masses make the interpretation of the results rather difficult. Irrespective to the size of the nonresonant contribution, a proper formulation for this amplitude is in order.

In this paper, a new approach for the decay amplitude is presented, as an alternative to the isobar model. The formalism is applicable to decays of charged mesons – D^+, D_s^+ and B^+ – into three kaons. These decays may proceed through a common topology: the annihilation diagram, in the language of the quark diagrammatic approach proposed by Chau[2].

In this specific topology, the decay amplitude may be written as

$$\mathcal{A} = \langle (KKK)^+ | A_\mu | 0 \rangle \langle 0 | A_\mu | M^+ \rangle$$

where A_μ is the axial weak current. The second term in the right-hand side corresponds to the weak vertex and depends on the quark content of the initial meson M^+. The firt term of the decay amplitude, $\langle (KKK)^+ | A_\mu | 0 \rangle$, hereafter referred to as the Multi-Meson Model, or Triple-M, has an universal character, and is the main subject of this work.

This paper is focused, without any loss of generality, on the $D^+ \to K^- K^+ K^+$ decay, for which the annihilation diagram is expected to be the dominant mechanism. Other possible topologies for this decay involve rescattering, and will be the subject of a future publication. The formalism can be easily extended to the decays of the D_s^+ and B^+ mesons, together with other topologies that must be considered.

The Triple-M amplitude contains three components: $(KKK)^+$ nonresonant, the $f_0(980)K^+$ and ϕK^+, derived from a chiral effective theory and dressed with coupled channels where appropriate.

In the Triple-M amplitude, the relative contribution and phase of each component is fixed by theory, and this represent an important difference with the isobar model. There are only three parameters in the Triple-M related to the mass of f_0 and its couplings to light pseudoscalars. At present, the values of these parameters are estimated by theory but, ultimately, they should be determined by fits to the data.

The model, in its present version, does not include three-body final state interactions (FSI). These FSI have been shown to play a significant role in the $D^+ \to K^- \pi^+ \pi^+$ decay [3–7] where the three-body unitarity was implemented differently by using Faddeev-like decomposition[3, 5], Kuri-Trieman equation[6] and triangle diagrams [7]. Although the inclusion of the three-body FSI is necessary for a complete description of the decay process, it brings new complex loop structures that increase significantly the computation.

The main purpose of this work is the identification of the leading structures acting in $D^+ \to K^+ K^- K^+$ decay to be applied to the data as an alternative to isobar model and it is organized as follows. The Triple-M amplitude is discussed in sections II to IV and the suggested amplitude for data fitting is given in section V. Some simulations and general remarks are given in section VI. Details of the calculations are given in the appendices.

II. MODEL

In the study of heavy meson decays, one deals with matrix elements of both vector and axial currents between hadronic states. Usually, the structure of these matrix elements is parametrized in terms of form-factors and their shapes tend to be associated with resonances.

At low energies, one deals mostly with matrix elements involving single particle states, which have been widely considered in the literature. However, in the case of some leptonic reactions and heavy meson decays, available energies can be large enough for allowing the simultaneous production of several pseudoscalars. Proper multi-meson structures become then relevant. For instance, the process $e^-\,e^+ \to 4\,\pi$ involves the matrix element $\langle \pi\pi\pi\pi | J^\mu_\gamma | 0 \rangle$, J^μ_γ being the electromagnetic current [8]. A similar matrix element, with J^μ_γ replaced with the weak current $(V-A)^\mu$, is instrumental to the description of the decay $\tau \to \nu\, 4\pi$ [8].

In the case of D and B hadronic decays, a rich structure of multi-meson final states has been identified in the large amount of recent data. Theoretical descriptions of these decays involve two distinct sets of interactions. The first one concerns the primary weak vertex, in which a heavy quark, either c or b, emits a W and becomes a $SU(3)$ quark. As this process happens within the heavy meson, it corresponds to the effective decay of a D or a B into a first set of $SU(3)$ mesons. This is followed by purely hadronic final state interactions, in which the mesons produced in the weak decay rescatter, before being detected. As both weak and final state interactions include several competing processes, the treatment of heavy meson decays into hadrons is necessarily involved.

One usually begins with the topologies given by Chau [2], which implement CKM quark mixing for processes based on a single W. Actual calculations, however, require the incorporation of Chau's scheme into effective hadronic descriptions. A possibility is to use factorization, as in the work of Bauer, Stich and Wirbel [9]. Or alternatively, one can depart from effective Lagrangians [10].

As instances, one mentions recent studies of the decay $D^+ \to K^-\pi^+\pi^+$. Processes based on the axial current require the product of matrix elements $\langle \pi^+ | A^\mu | 0 \rangle \langle \pi^+ K^- | A_\mu | D^+ \rangle$ [11], whereas those emphasizing the vector current rely on the product $\langle \pi^+\pi^+ K^- | V^\mu | \bar{K}^0 \rangle \langle \bar{K}^0 | V_\mu | D^+ \rangle$, with the $\bar{K}^0$ kept inside a loop [3, 4].

In the present work, we concentrate on effects associated with the matrix element $\langle K^-\, K^+\, K^+ | A^\mu |\, 0 \,\rangle$, which is especially relevant for the decay $D^+ \to K^-\, K^+\, K^+$.

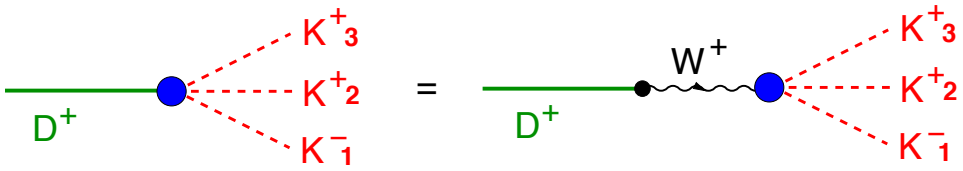

FIG. 1: The decay $D^+ \to K^- K^+ K^+$ (left) is assumed to proceed thought quark-annihilation topology in the steps $D^+ \to W^+$ and $W^+ \to K^- K^+ K^+$ (right).

We assume the decay to be dominated by the process shown in Fig. 1 and determine the multi-meson matrix element by means of chiral effective theories. The motivation for chiral symmetry is that the u-, d-, and s-quark masses are small when compared with the QCD scale $\Lambda \sim 1\,\mathrm{GeV}$, indicating that the light sector of the theory is not far from the massless limit, which is symmetric under the chiral $SU(3) \times SU(3)$ flavour group. In this approach, light-quark condensates are included naturally and pseudoscalar mesons are Goldstone bosons. The *Chiral Perturbation Theory* was originally designed to describe low-energy interactions [12, 13], where it yields the most reliable representation of the Standard Model. Its scope was later enlarged, with the inclusion of resonances as chiral corrections [14], coupling schemes suited for heavy mesons [10], and partial unitarization, by means of diagram ressummations [15].

Here, one is concerned just with the simplest possible structures, which could be instrumental to empirical data analyses. We work within the K-matrix approximation and, therefore, skip loop contributions from off-shell states. Our results are compatible with the conservation of the vector current (CVC) and partial conservation of the axial current (PCAC). The latter is especially relevant for this problem, since it implies that the divergence of the axial current is proporcional to M_K^2.

III. TREE-LEVEL AXIAL CURRENTS

The decay $D^+(P) \to K^-(p_1)\, K^+(p_2)\, K^+(p_3)$ is assumed to proceed thought the intermediate steps $D^+ \to W^+$ and $W^+ \to K^- K^+ K^+$, as in Fig. 1. The former is associated with the matrix element

$$\langle\, 0\,|A^\mu|\, D^+(P)\rangle = -i\,\sqrt{2}\,F_D\,P^\mu\,, \tag{1}$$

where F_D is a constant and $P = (p_1 + p_2 + p_3)$.

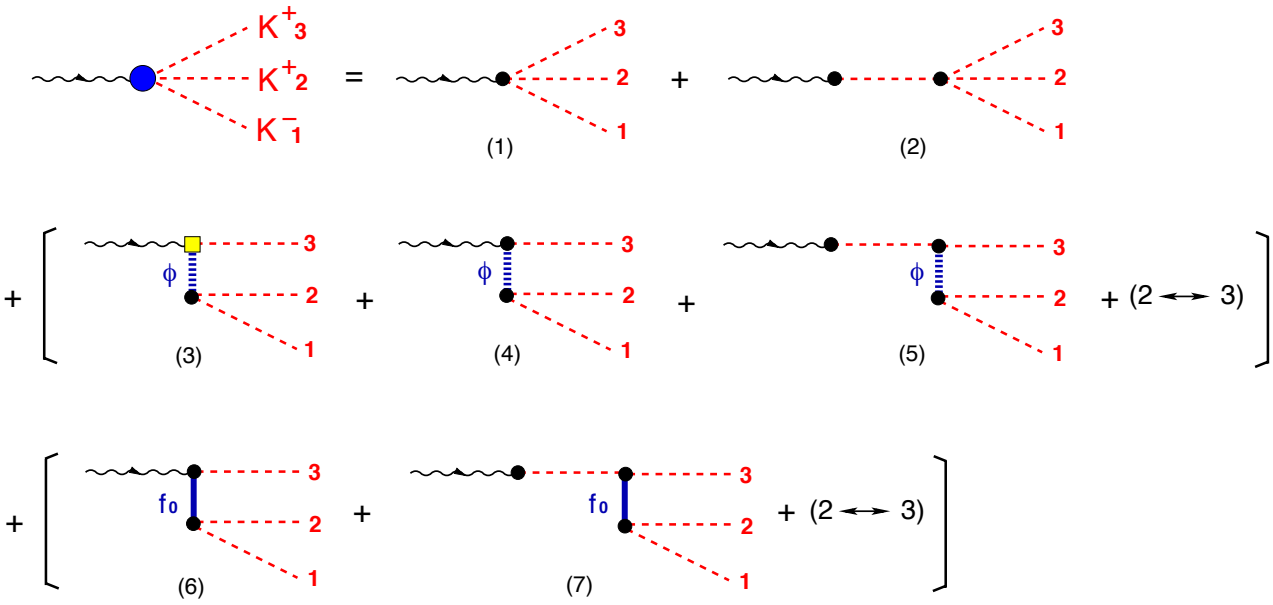

FIG. 2: Tree-level structure for the $A^\mu \to K^- K^+ K^+$ matrix element: the top line is LO and terms within brackets, which involve ϕ and f_0 intermediate states, are NLO; there are two different forms for the $WK\phi$ coupling, indicated by a yellow box and a black dot.

This work relies heavily on the chiral effective lagrangians including resonances, developed by Ecker, Gasser, Pich and De Rafael [14], where the formalism needed can be found. In particular, one follows their conventions for coupling constants. The tree-level matrix element $\langle K^-(p_1)\, K^-(p_2)\, K^+(p_3)|A^\mu|\, 0\,\rangle$ is given in Fig. 2, where the top line displays the leading order (LO) contact terms, whereas NLO corrections are given within brackets. Individual contributions are given in Appendix E. The full contact term term $(1)+(2)$ includes a kaon pole and can be written as

$$\langle K^-(p_1)\, K^+(p_2)\, K^+(p_3)|A^\mu|\, 0\,\rangle_{(c)} = -i \left[\frac{2\sqrt{2}}{F_K}\right] \frac{1}{P^2 - M_K^2}$$
$$\times \left\{ \left[P^2\,(p_2+p_3)^\mu - P\cdot(p_2+p_3) P^\mu\right] + M_K^2\, p_1^\mu \right\} \ , \qquad (2)$$

where F_K is the kaon decay constant.

The treatment of the ϕ-meson includes the $\pi\pi\pi$ intermediate channel. This contribution is assumed to be saturated by $\rho\pi$ intermediate states and is already included into the ϕ propagators in Fig. 2. The structure of this dressed propagator, denoted by $[D_\phi^{\pi\rho}]^{-1}$, is discussed in Appendix B and given by eq. (B18). The ϕ contribution involves two independent

terms, namely (3) and (4) + (5), and reads

$$
\begin{aligned}
&\langle K^-(p_1)K^+(p_2)K^+(p_3)|A^\mu|\,0\,\rangle_{(\phi)} \\
&= -i\,\left[\sin^2\theta\,\frac{3\,\sqrt{2}\,F_V\,G_V}{2\,F_K^3}\right]\,\frac{[P{\cdot}p_2\,p_1^\mu - P{\cdot}p_1\,p_2^\mu]}{D_\phi^{\pi\rho}(m_{12}^2)} \\
&+i\,\left[\sin^2\theta\,\frac{3\,\sqrt{2}\,G_V^2}{F_K^3}\right]\,\frac{1}{P^2-M_K^2}\,\left\{\frac{1}{D_\phi^{\pi\rho}(m_{12}^2)}\right. \\
&\times\left[p_2{\cdot}p_3\,\left(P^2\,p_1^\mu - P{\cdot}p_1\,P^\mu\right) - p_1{\cdot}p_3\,\left(P^2\,p_2^\mu - P{\cdot}p_2\,P^\mu\right)\right. \\
&\left.\left.-M_K^2\,\left(p_2{\cdot}p_3\,p_1^\mu - p_1{\cdot}p_3\,p_2^\mu\right)\right]\right\} + (2\leftrightarrow 3)\;, \qquad (3)
\end{aligned}
$$

where θ is the $\omega-\phi$ mixing angle and F_V and G_V are coupling constants defined in Ref. [14].

As the role of the scalar $f_0(980)$ in the $SU(3)$ structure is not clear, we allow it to be either a singlet or a member of an octet (hereafter we refer to $f_0(980)$ only as f_0). In the formal developments, these two possibilities are labelled by (0) and (8), respectively, and treated together as long as possible. The terms (6) + (7) of Fig. 2 yield

$$
\begin{aligned}
&\langle K^-(p_1)K^+(p_2)K^+(p_3)|A^\mu|\,0\,\rangle_{(f_0)} \\
&= i\,\left[\gamma_n\,\frac{\sqrt{2}}{3\,F_K^3}\right]\,\frac{1}{P^2-M_K^2}\,\left\{\frac{1}{m_{12}^2-m_{f_0}^2}\right. \\
&\times\left[c_d\,(P^2\,p_3^\mu - P{\cdot}p_3\,P^\mu) - M_K^2(c_d\,p_3^\mu - c_m\,P^\mu)\right] \\
&\left.\times\left[c_d\,m_{12}^2 - 2\,(c_d-c_m)\,M_K^2\right] + (2\leftrightarrow 3)\right\}\;, \qquad (4)
\end{aligned}
$$

where c_d and c_m are coupling constants (black dots in diagrams (6) and (7) in Fig. 2) [14], and we have used $\tilde{c}_i = c_i/\sqrt{3}$ for the singlet, and $\gamma_0 = 8$ and $\gamma_8 = 1$.

The decay amplitude of the D^+, given in Fig. 1, is

$$
T = \left[\frac{G_F}{\sqrt{2}}\,\sin^2\theta_C\right]\,\sqrt{2}\,F_D\,\left[i\,P_\mu\,\langle K^-(p_1)K^+(p_2)K^+(p_3)|A^\mu|\,0\,\rangle\right]\;, \qquad (5)
$$

where θ_C is the Cabibbo angle and G_F is the Fermi weak constant.

Structures of the form $(P{\cdot}y\,x^\mu - P{\cdot}x\,y^\mu)$, for two generic vectors x^μ and y^μ, vanish when multiplied by P_μ and the multi-meson current divergence is proportional to M_K^2, as expected by PCAC. In terms of the form factors proposed by Kühn and Mirkes [16], this means that

the decay amplitude is proportional to their F_4. Results (2-4) yield the tree contribution

$$
\begin{aligned}
T_{tree} = C \; \Big\{ & \left[M_D^2 + M_K^2 - m_{23}^2 \right] \\
& - \left[\sin^2\theta \, \frac{3\, G_V^2}{4 F_K^2} \right] \left[\frac{m_{12}^2}{D_\phi^{\pi\rho}(m_{12}^2)} \; \left(m_{13}^2 - m_{23}^2 \right) + 2 \leftrightarrow 3 \right] \\
& - \left[\frac{\gamma_n}{6 \; F_K^2} \right] \left[\frac{1}{m_{12}^2 - m_{f_0}^2} \left[c_d \; \left(m_{12}^2 - M_K^2 \right) - \left(c_d - 2\, c_m \right) M_D^2 \right] \right. \\
& \left. \times \left[c_d \, m_{12}^2 - 2 \left(c_d - c_m \right) M_K^2 \right] + 2 \leftrightarrow 3 \right] \Big\} \; . \qquad (6)
\end{aligned}
$$

where C is the constant

$$
C = \left[\frac{G_F}{\sqrt{2}} \, \sin^2\theta_C \right] \, \frac{2 F_D}{F_K} \, \frac{M_K^2}{M_D^2 - M_K^2} \; . \qquad (7)
$$

The factor C has dimension $[m]^{-2}$, given by the Fermi constant $G_F = 1.166 \times 10^{-5}\,\mathrm{GeV}^{-2}$.

IV. FINAL STATE INTERACTIONS

The full amplitude is obtained by including final state interactions in the processes of Fig. 2. Here we consider only two-body rescattering process, leaving the three-body treatment to a future work. The corresponding dynamics is described in Fig. 3 and involves two classes of contributions. The first one, shown by diagrams (1a) and (2a), concerns $\bar{K}K$ rescattering. In principle, the intermediate states could have isospin $I = 0, 1$ and angular momentum $J = 0, 1$. We keep only contributions with $I = 0, J = 1$, associated with the ϕ channel, and postpone the discussion of the other ones. The second class corresponds to employing the production amplitudes, derived in Appendix D, which endow the ϕ and f_0 propagators with their full widths.

The nonresonant contribution is determined at tree-level. Dynamically, it is a proper three-body amplitude, a direct consequence of chiral symmetry, which predicts multi-meson topologies. This goes beyond the notion of a spectator particle, as in the 2+1 approximation (two-body subsystem+spectator). It is given by a real polynomial, which can be written in two alternative forms

$$
T_{NR} = C \; \left[\, M_D^2 + M_K^2 - m_{23}^2 \, \right] \; , \qquad (8)
$$

$$
= C \; \left[\, (m_{12}^2 - M_K^2) \, + 2 \leftrightarrow 3 \, \right] \; . \qquad (9)
$$

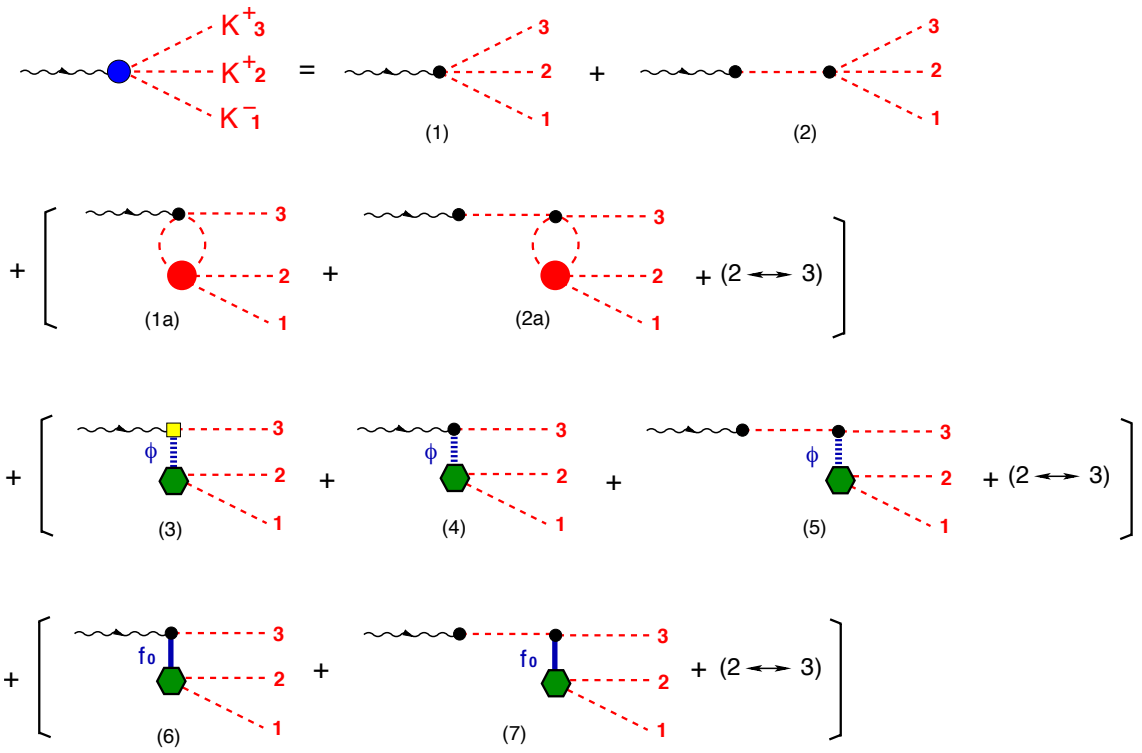

FIG. 3: Dynamical structure of the $A^\mu \to K^- K^+ K^+$ matrix element, including final state interactions: the top line, diagrams (1) and (2), is the LO nonresonant contribution, diagrams (1a) and (2a) include a KK rescattering, indicated by the red blob; whereas diagrams (3-7) describe ϕ and f_0 contributions with their full widths; there are two different forms for the $WK\phi$ coupling, indicated by a yellow box and a black dot.

The second form makes it clear that T_{NR} contains just S-waves.

The rescattering amplitudes, given by diagrams $(1a + 2a)$ in Fig. 3, involve intermediate states with the same quantum numbers as the f_0 and the ϕ, which are denoted by T_{Rf} and $T_{R\phi}$. We postpone the discussion of the former and next, we consider the latter, together with the ϕ contribution T_ϕ, associated with diagrams $(3 + 4 + 5)$ and based on results from Appendices C and D. They read

$$T_{R\phi} = -i\,C\,\left[\sin^2\theta\,\frac{3\,G_V^2}{4F_K^2} - \frac{3\,D_\phi^{\pi\rho}}{8\,m_{12}^2}\right]\,\left[\frac{m_{12}\,[Q_c^3 + Q_n^3]}{16\pi\,F_K^2}\,\frac{[m_{13}^2 - m_{23}^2]}{D_\phi(m_{12}^2)} + 2 \leftrightarrow 3\right]\,, \qquad (10)$$

$$T_\phi = -C\,\left[\sin^2\theta\,\frac{3\,G_V^2}{4F_K^2}\right]\,\left[m_{12}^2\,\frac{[m_{13}^2 - m_{23}^2]}{D_\phi(m_{12}^2)} + 2 \leftrightarrow 3\right]\,, \qquad (11)$$

where

$$D_\phi(s) = s - m_\phi^2 + i\, m_\phi\, \Gamma_\phi(s) - \left[i\, \frac{1}{8\pi\, F_K^2}\, \frac{D_\phi^{\pi\rho}(s)}{\sqrt{s}}\, \left(Q_c^3 + Q_n^3\right) \right] , \tag{12}$$

$$m_\phi\, \Gamma_\phi(s) = \sqrt{s}\, \left[\Gamma_{KK}\, \frac{(Q_c^3 + Q_n^3)}{(\tilde{Q}_c^3 + \tilde{Q}_n^3)} + \Gamma_{\pi\rho}\, \frac{s}{m_\phi^2}\, \frac{Q_{\pi\rho}^3}{\tilde{Q}_{\pi\rho}^3} \right] , \tag{13}$$

$$D_\phi^{\pi\rho}(s) = s - m_\phi^2 + i\, \Gamma_{\pi\rho}\, \frac{s^{3/2}}{m_\phi^2}\, \frac{Q_{\pi\rho}^3}{\tilde{Q}_{\pi\rho}^3} . \tag{14}$$

with $Q_{\pi\rho} = \frac{1}{2}\sqrt{s - 2\,(M_\pi^2 + m_\rho^2) + (M_\pi^2 - m_\rho^2)^2/s}$, $Q_c = \frac{1}{2}\sqrt{s - 4M_{K^+}^2}$, $Q_n = \frac{1}{2}\sqrt{s - 4M_{K^0}^2}$ and $\tilde{Q} = Q(s = m_\phi^2)$. In Eq.(13), $\Gamma_{\pi\rho}$ and Γ_{KK} are the decay width of the ϕ and their values can be found in PDG [17]. The use made of Γ_{KK} fixes the ϕ coupling constant, as in eq.(C33), to be

$$\sin^2\theta\, \frac{3\, G_V^2}{4\, F_K^2} = \frac{3\pi\, F_K^2\, \Gamma_{KK}}{(\tilde{Q}_c^3 + \tilde{Q}_n^3)} . \tag{15}$$

The functions $T_{R\phi}$ and T_ϕ share the same dressed ϕ propagator, owing to the presence of the $\bar{K}K$ amplitude in the former.

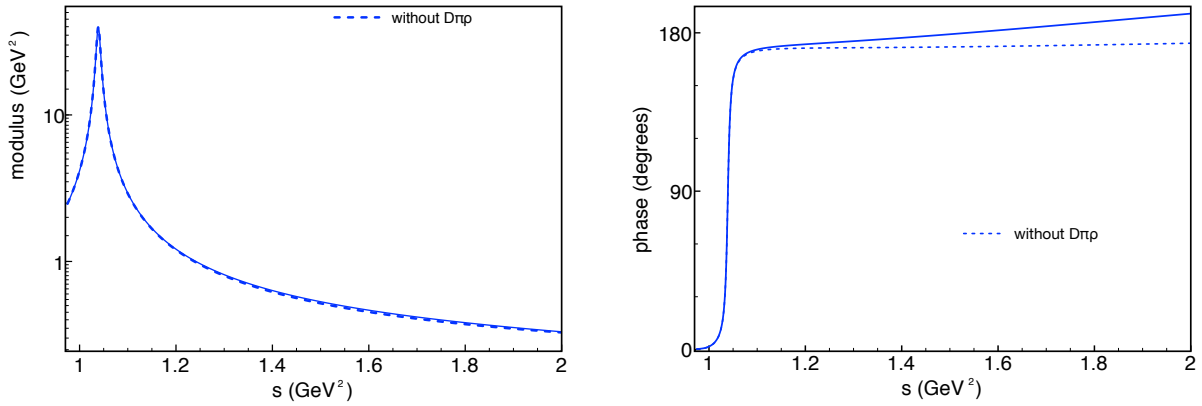

FIG. 4: Moduli (left) and phases (right) of the ratio $[T_{R\phi} + T_\phi]/[-C\,(m_{13}^2 - m_{23}^2)]$, eqs.(10) and (11), with (continuous blue) and without (dotted blue) the factor $D_\phi^{\pi\rho}$, eq.(14).

Our results contain several new features. One of them regards the description of intermediate $\bar{K}K$ interactions, which rely on contributions from both resonances and pont-like processes, as discussed in Appendix C. The latter vanish at the peak of the resonance and increase as one moves away from it. Their signature are the terms proportional to $D_\phi^{\pi\rho}$. In Fig. 4, we assess the importance of intermediate contact interactions, by comparing results

for the dimensionless ratio $[T_{R\phi}+T_\phi]/[-C\,(m_{13}^2-m_{23}^2)]$, with and without $D_\phi^{\pi\rho}$. One learns that contact interactions have little numerical relevance in the phase-space accessible to the $D^+\to K^+K^-K^+$ decay.

In Fig. 5 we display the relative importance of the ratios $T_{R\phi}/[-C\,(m_{13}^2-m_{23}^2)]$ and $T_\phi/[-C\,(m_{13}^2-m_{23}^2)]$, and notices that the latter is largely dominant. The dip on the curve associated with $T_{R\phi}$, around $s=1.8\,\mathrm{GeV}$, is due to the destructive interference between the two terms in the first bracket of eq.(10) in that region.

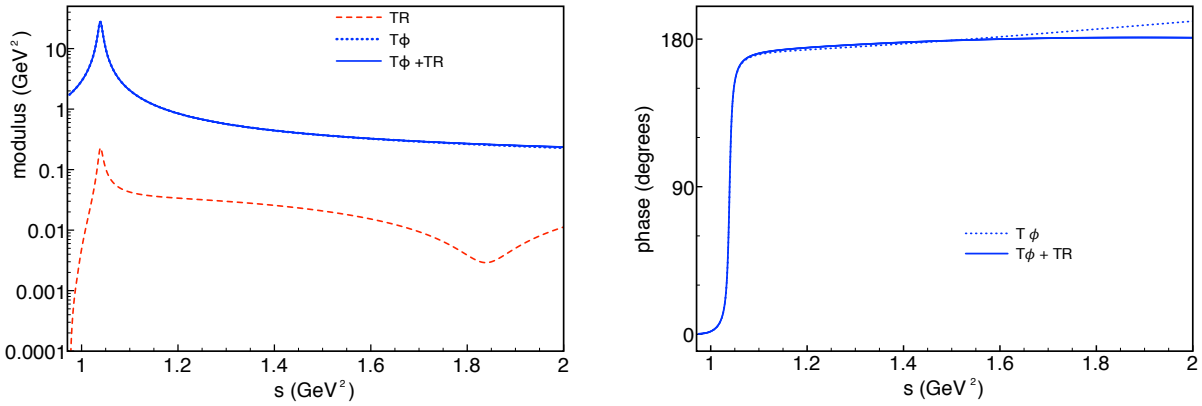

FIG. 5: Moduli(left) and phases(right) of $T_{R\phi}/[-C\,(m_{13}^2-m_{23}^2)]$, eq.(10) (dashed red), $T_\phi/[-C\,(m_{13}^2-m_{23}^2)]$, eq(11) (dotted blue) and $[T_\phi+T_R]/[-C\,(m_{13}^2-m_{23}^2)]$ (continuous blue).

The preceding discussion indicates that, in the ϕ channel, both $D_\phi^{\pi\rho}$ and $T_{R\phi}$ contributions are small and, for the sake of simplicity, they can be safely removed from the model. Another new feature in our results concerns the independent widths for K^-K^+, $\bar{K}^0K^0$, and $\rho\pi$ decay modes, which give rise to the structures proportional to Q_c, Q_n and $Q_{\pi\rho}$ in eq.(13). A last issue is the factor m_{12}^2 in the numerator of eq.(11), and the $\sqrt{s}$ outside the bracket in eq.(13), which are signatures of resonance couplings in chiral perturbation theory. Thus, the leading contribution in the ϕ-channel is proportional to the dimensionless function

$$A_{TM\phi}=\frac{s}{s-m_\phi^2+i\,m_\phi\,\Gamma_{TM\phi}}\,, \tag{16}$$

with $m_\phi\,\Gamma_{TM\phi}$ given by eq.(13). In Fig. 6, we compare it with the usual relativistic Breit-Wigner (BW) [1] for the same channel, employed in most Dalitz plot analyses, excluding barrier and spin factors, which reads

$$A_{BW\phi}=\frac{m_\phi^2}{s-m_\phi^2+i\,m_\phi\,\Gamma_{BW\phi}} \tag{17}$$

$$m_\phi\,\Gamma_{BW\phi}(s) = \Gamma_\phi\left[\frac{m_\phi^2}{\sqrt{s}}\right]\,\frac{Q_c^3(s)}{\tilde{Q}_c^3}\,, \tag{18}$$

$$\Gamma_\phi = \Gamma_{KK} + \Gamma_{\pi\rho}\,, \tag{19}$$

The factor m_ϕ^2 in the numerator of eq.(17) was introduced so that it has the same normalization as eq.(16), at the pole. The main differences between both expressions are the factors proportional to s/m_ϕ^2, associated with chiral symmetry. Their effects are already visible at $s \sim 1.2\,\mathrm{GeV}$ and increase with energy. In particular it is interesting to note that the modulus of the BW falls faster than that of the Triple-M at high values of s.

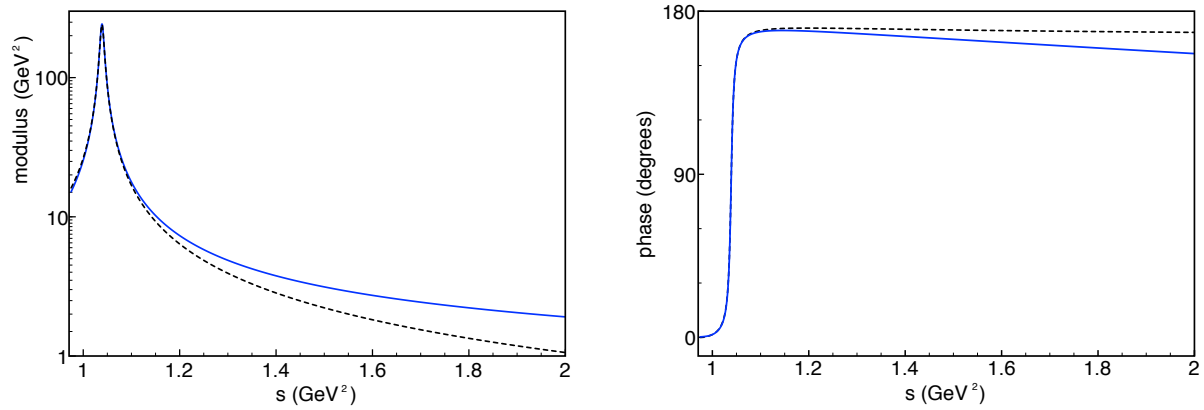

FIG. 6: Moduli (left) and phases (right) of the functions $A_{TM\phi}$, eq.(16), (continuous blue) and $A_{BW\phi}$, eq.(17), (dashed black).

The $SU(3)$ status of the f_0 is uncertain and, for instance, one could follow Ref. [14], assuming it to be a linear combination of singlet and octet states. However, owing to the exploratory nature of this work, we consider it to be either a singlet or an octet, labelled by subscripts (0) and (8). These possibilities affect both the intensity of the f_0 coupling and the relative proportion of $\pi\pi$ and $\bar{K}K$ in its decay modes. The two alternatives are written as

$$T_{f_0} = -C\left[\frac{\gamma_n}{6F_K}\right]\,\left[\left[c_d\,\left(m_{12}^2 - M_K^2\right) - \left(c_d - 2\,c_m\right)M_D^2\right]\,\frac{G_K(m_{12}^2)}{D_n(m_{12}^2)} + 2 \leftrightarrow 3\right]\,, \tag{20}$$

with $\gamma_0 = 8\,,\ \gamma_8 = 1\,,$ and

$$D_n(s) = s - m_{f_0}^2 + i\,m_{f_0}\,\Gamma_n(s)\,, \tag{21}$$

$$m_{f_0}\,\Gamma_0 = \frac{G_\pi^2}{4\pi F_\pi^2}\,\frac{Q_{\pi\pi}}{\sqrt{s}} + \frac{G_K^2}{3\pi F_K^2}\,\frac{Q_{KK}}{\sqrt{s}} + \frac{G_\eta^2}{12\pi F_\eta^2}\,\frac{Q_{\eta\eta}}{\sqrt{s}}\,\Theta[s - 4\,M_\eta^2]\,, \tag{22}$$

$$m_{f_0}\,\Gamma_8 = \frac{G_\pi^2}{8\pi F_\pi^2}\,\frac{Q_{\pi\pi}}{\sqrt{s}} + \frac{G_K^2}{24\pi F_K^2}\,\frac{Q_{KK}}{\sqrt{s}} + \frac{G_\eta^2}{24\pi F_\eta^2}\,\frac{Q_{\eta\eta}}{\sqrt{s}}\,\Theta[s-4\,M_\eta^2]\;, \tag{23}$$

$$G_P(s) = \frac{[c_d\,s - 2\,(c_d - c_m)\,M_P^2]}{F_P}\;, \tag{24}$$

$$Q_{PP}(s) = \frac{1}{2}\sqrt{s-4\,M_P^2}\;, \tag{25}$$

for $P = \pi, K, \eta$.

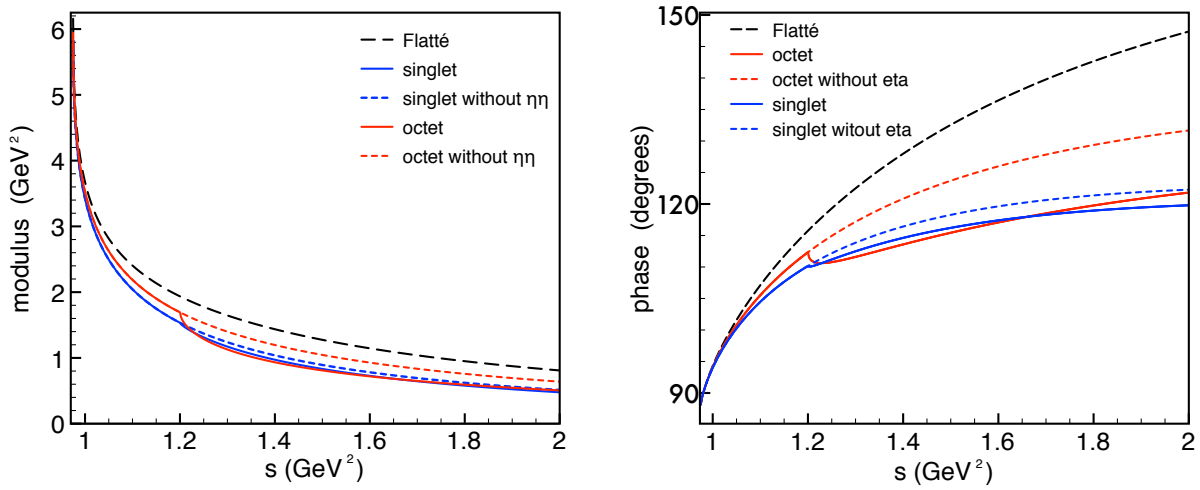

FIG. 7: Moduli(left) and phases(right) of the dimensionless amplitudes A_{Flatte}, eq.(27) (dashed black) and $A_{TM\,f_0}$, eq.(26) for the singlet (continuous blue) and octet (continuous red) cases; the cusps in the last two curves are due to the opening of the $\eta\eta$ channel; the elimination of this coupling gives rise to the corresponding dashed curves.

For the sake of completeness, we have allowed the f_0 to couple to an intermediate $\eta\eta$ state, even if it becomes relevant at higher energies only. The most striking feature of the f_0 in the Triple-M is the presence of s-dependent couplings, predicted by chiral perturbation theory [14]. This means that the amplitude T_{f_0} is somewhat flexible, since it depends on two free coupling parameters, namely c_d and c_m. In Fig. 7, we compare the dimensionless functions

$$A_{TM\,f_0} = \frac{m_{f_0}^2}{s - m_{f_0}^2 + i\,m_{f_0}\,\Gamma_n(s)}\;, \tag{26}$$

for $n = 0,\,8$, eqs.(22) and (23), with a Flatté function [18], with parameters obtained by BES from $J/\psi \to \phi\pi\pi(K\,K)$ data [$g_{\pi\pi} = 0.165\,\mathrm{GeV}$ and $g_{KK} = 0.695\,\mathrm{GeV}$] [19]

$$A_{Flatte} = \frac{m_{f_0}^2}{s - m_{f_0}^2 + i\,m_{f_0}\,2\,[g_{\pi\pi}\,Q_{\pi\pi} + g_{KK}\,Q_{KK}]\,/\sqrt{s}}. \tag{27}$$

In order to make the comparison meaningful, we fix the parameters c_d and c_m in eq.(26) so that A_{TMf_0} and A_{Flatte} have the same modulus at $s = m_{f_0}^2$. This yields $[c_d,\, c_m = 0.016,\, 0.069\,]\,\mathrm{GeV}$, for the singlet, and $[c_d,\, c_m = 0.018,\, 0.220\,]\,\mathrm{GeV}$, for the octet. Inspecting figure 7, one notes that effect of the $\eta\eta$ channel manifest as threshold cusps around $s \sim 1.2\,\mathrm{GeV}$ and remain visible afterwards. Even when the $\eta\eta$-coupling is neglected, the differences between the Flatté function and Triple-M predictions remain important.

The dependence of T_{f_0}, eq.(20), on the free parameters c_d and c_m is a rather strong one. This is illustrated in Fig. 8, where we display our singlet and octet predictions for the ratio $T_{f_0}/[-C]$, based on the choices used in Fig. 7, without the $\eta\eta$-coupling, together with those obtained by using the values proposed by Ecker, Gasser, Pich e Rafael[14], namely $[c_d,\, c_m = 0.032,\, 0.042\,]\,\mathrm{GeV}$. It is clear that the values of c_d and c_m can affect considerably the final line shape of the f_0 and one is entitled to expect fits to data to be quite sensitive to these parameters.

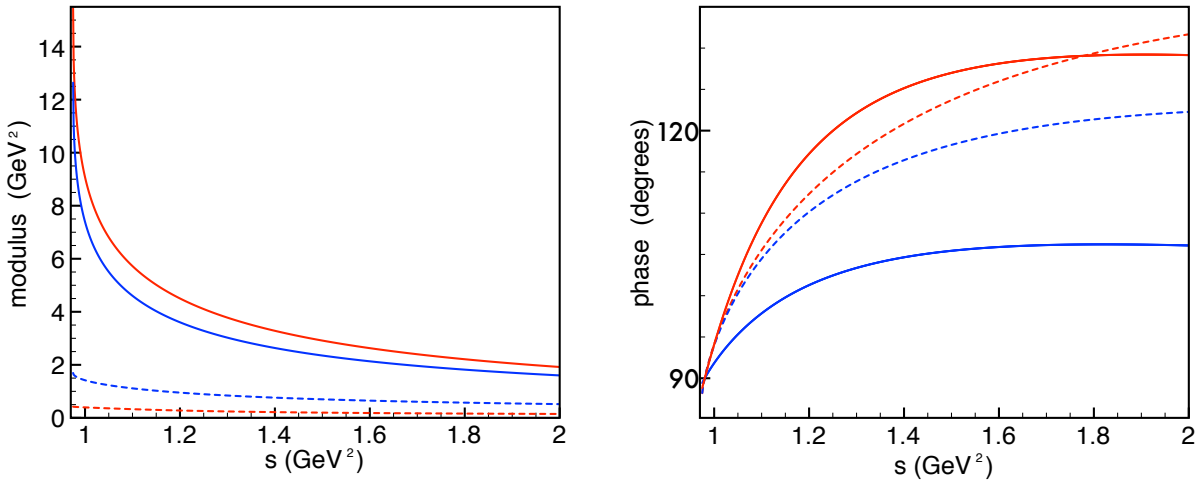

FIG. 8: Moduli(left) and phases(right) of the ratio $T_{f_0}/[-C]$, eq.(20) for the singlet (blue curves) and octet (red curves) cases, based on the same values of c_d and c_m as in Fig. 7 (continuous curves) and on those given in Ref. [14] (dashed curves).

In the Triple-M, the S-wave receives contributions from both T_{NR}, and T_{f_0}. Their relative importance is assessed in Fig. 9, where we display the ratios $T_{NR}/[-C]$, eq.(9), $T_{f_0}/[-C]$, eq.(20), and their sum, using the parameters c_d and c_m fixed by the Flatté function, eq.(27). The figure indicates that the interference of these two terms is mostly destructive. The f_0 dominates at low energies whereas the nonresonant interaction increase linearly with

the energy. The resulting profile for the modulus of the S-wave falls from threshold up to $s \sim 2\,\mathrm{GeV}$, where it has a minimum. This pattern of interference is also important for the phase.

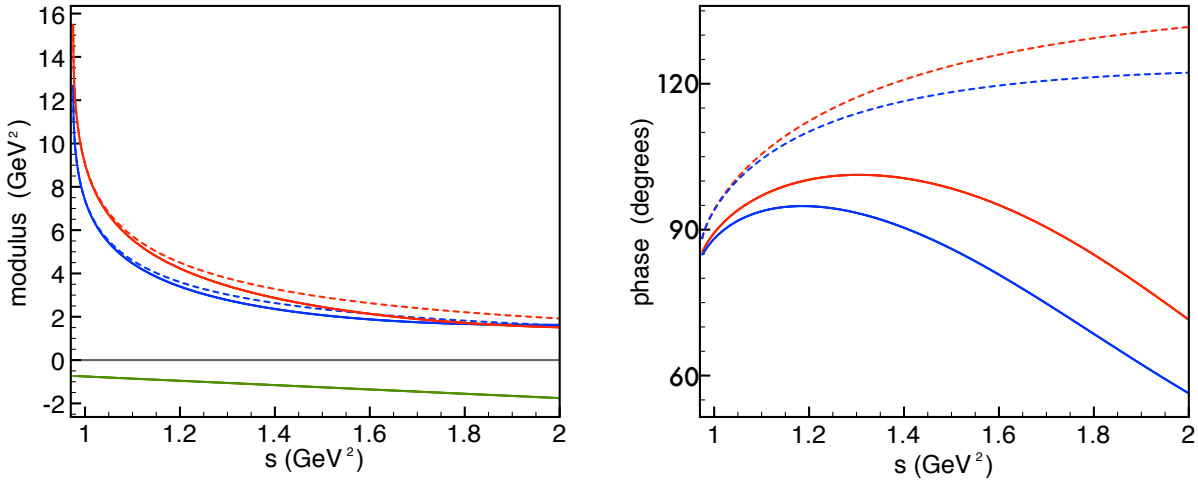

FIG. 9: Moduli(left) and phases(right) for the dimensionless ratios $T_{NR}/[-C]$, eq.(9), (continuous green), $T_{f_0}/[-C]$, eq.(20), for the singlet (dashed blue) and octet (dashed red) cases, together with their sums (continuous blue and red).

V. THE MULTI-MESON MODEL - TRIPLE-M

The main purpose of this work is to provide a reliable model to be used for fitting data. Our full results incorporate the dynamics described in Fig. 3 and the corresponding mathematical expressions were given in the previous section, where the leading contributions of each kind were identified. Here, we present a simplified version of the Triple-M amplitude, composed by these leading contributions, which contain three free parameters, associated to the scalar f_0. Our Triple-M amplitude include a nonresonant contribution (NR), supplemented by ϕ and f_0 resonant terms, and is formally written as

$$T_{_{MMM}} = T_{NR} + T_{\phi} + T_{f_0} \ , \tag{28}$$

The nonresonant term is given directly from diagrams $(1+2)$ in Fig. 3 and reads

$$T_{NR} = C \ \left\{ M_D^2 + M_K^2 - m_{23}^2 \right\} \ , \tag{29}$$

where C is the constant with dimension $[m]^{-2}$, given in eq.(7)

$$C = \left[\frac{G_F}{\sqrt{2}}\,\sin^2\theta_C\right]\,2\,\frac{F_D}{F_K}\,\frac{M_K^2}{M_D^2 - M_K^2}\,.$$

The amplitude $T_{R\phi}$, eq.(10), is neglected and the ϕ contribution is

$$T_\phi = -C\,\left[\sin^2\theta\,\frac{3\,G_V^2}{4F_K^2}\right]\,\left[m_{12}^2\,\frac{[m_{13}^2 - m_{23}^2]}{D_\phi(m_{12}^2)} + 2 \leftrightarrow 3\right]\,, \tag{30}$$

with

$$D_\phi(s) = s - m_\phi^2 + i\,m_\phi\,\Gamma_\phi(s)\,, \tag{31}$$

$$m_\phi\,\Gamma_\phi(s) = \sqrt{s}\,\left[\Gamma_{KK}\,\frac{(Q_c^3 + Q_n^3)}{(\tilde{Q}_c^3 + \tilde{Q}_n^3)} + \Gamma_{\pi\rho}\,\frac{s}{m_\phi^2}\,\frac{Q_{\pi\rho}^3}{\tilde{Q}_{\pi\rho}^3}\right]\,. \tag{32}$$

There are no free parameters in T_ϕ. The partial widths are $\Gamma_{KK} = 3.55\,\mathrm{MeV}$ and $\Gamma_{\pi\rho} = 0.65\,\mathrm{MeV}$ [17]. Using the former in eq.(15), together with $F_K = 0.107\,\mathrm{GeV}$ [20], $\tilde{Q}_c = 126.41\,\mathrm{MeV}$, and $\tilde{Q}_n = 110.10\,\mathrm{MeV}$, one determines the coefficient of eq.(30) as

$$\sin^2\theta\,\frac{3\,G_V^2}{4\,F_K^2} = \frac{3\pi\,F_K^2\,\Gamma_{KK}}{(\tilde{Q}_c^3 + \tilde{Q}_n^3)} = 0.1140\,.$$

This expression also allows one to find the coupling constant G_V. The standard value $\sin\theta = 0.76$ [17] yields $G_V = 0.055\,\mathrm{GeV}$, which is quite close to the prescriptions from chiral perturbation theory [14] ($0.053\,-\,0.069\,\mathrm{GeV}$).

The amplitude T_{f_0} is obtained by neglecting $\eta\eta$ couplings:

$$T_{f_0} = -C\,\left[\frac{\gamma_n}{6F_K}\right]\,\left[\left[c_d\,\left(m_{12}^2 - M_K^2\right) - (c_d - 2\,c_m)\,M_D^2\right]\,\frac{G_K(m_{12}^2)}{D_n(m_{12}^2)} + 2 \leftrightarrow 3\right]\,, \tag{33}$$

$$D_n(s) = s - m_{f_0}^2 + i\,m_{f_0}\,\Gamma_n(s)\,, \tag{34}$$

$$m_{f_0}\,\Gamma_0 = \frac{G_\pi^2}{4\pi F_\pi^2}\,\frac{Q_{\pi\pi}}{\sqrt{s}} + \frac{G_K^2}{3\pi F_K^2}\,\frac{Q_{KK}}{\sqrt{s}}\,, \tag{35}$$

$$m_{f_0}\,\Gamma_8 = \frac{G_\pi^2}{8\pi F_\pi^2}\,\frac{Q_{\pi\pi}}{\sqrt{s}} + \frac{G_K^2}{24\pi F_K^2}\,\frac{Q_{KK}}{\sqrt{s}}\,. \tag{36}$$

The functions G_P, eq.(24), depend on the parameters F_P and, in the literature, one finds $F_\pi = 0.093\,\mathrm{GeV}$ [13], $F_K = 0.107\,\mathrm{GeV}$ [20]. The values of c_d and c_m are to be determined by fits to data and the low-energy estimates c_d, $c_m = 0.032$, $0.042\,\mathrm{GeV}$ [14] provide educated points of departure. For the propose of Monte-Carlo simulation, in the next section, we use the values obtained by comparing the f_0 width with Flatté function, as discussed in the previous section.

VI. MC SIMULATIONS

In this section, simulations of the Triple-M amplitude are presented for the decay $D^+ \to K^-(p_1)K^+(p_2)K^+(p_3)$. Note that the convention is that the odd-charged particle is always particle 1. Since the like-charged kaons are identical particles, the Dalitz plot is symmetric. This means $s_{12} \equiv (p_1 + p_2)^2$ and $s_{13} \equiv (p_1 + p_3)^2$ are equivalent. The third invariant, $s_{23} \equiv (p_2 + p_3)^2$, is the invariant mass squared of the two like-charged kaons. The Dalitz plots are represented in terms of s_{12} and s_{13} invariants. In this representation the s_{23} axis runs along the diagonal, with threshold $(4M_K^2)$ at the upper border of the Dalitz plot.

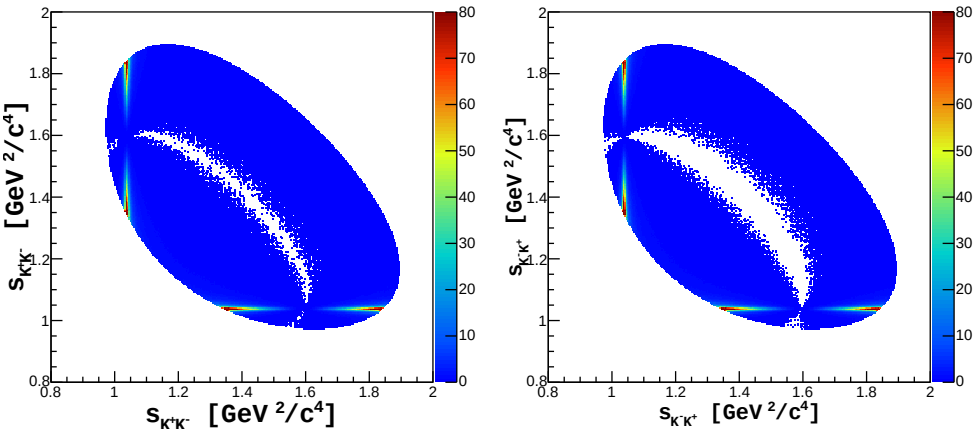

FIG. 10: Dalitz plot with the MC simulation of: a relativistic Breit-Wigner amplitude (left); the ϕ component of the Triple-M (right).

In Figs. 10 - 12, we present the results of a simulation to the $D^+ \to K^-K^+K^+$ Dalitz plot distribution for the individual components of the Triple-M amplitude. We compare our Triple-M simulation (plots on the right), with the corresponding amplitudes that are commonly used in Dalitz plot analyses (plots on the left): a relativistic Breit-Wigner, for the case of the ϕ, and the Flatté function, for the case of the f_0.

In the case of T_ϕ (Fig. 10), the Triple-M and the relativistic BW yield almost identical distributions. For the f_0, one found that the singlet and octet hypothesis yields nearly identical distributions, so only the singlet case is considered. A comparison between T_{f_0} and the Flatté function, made in Figs. 11, show that the two amplitudes result in a somewhat different distributions in the Dalitz plot. The T_{f_0} component yields a distribution which is more concentrated towards the threshold than that of the Flatté formula. The differences

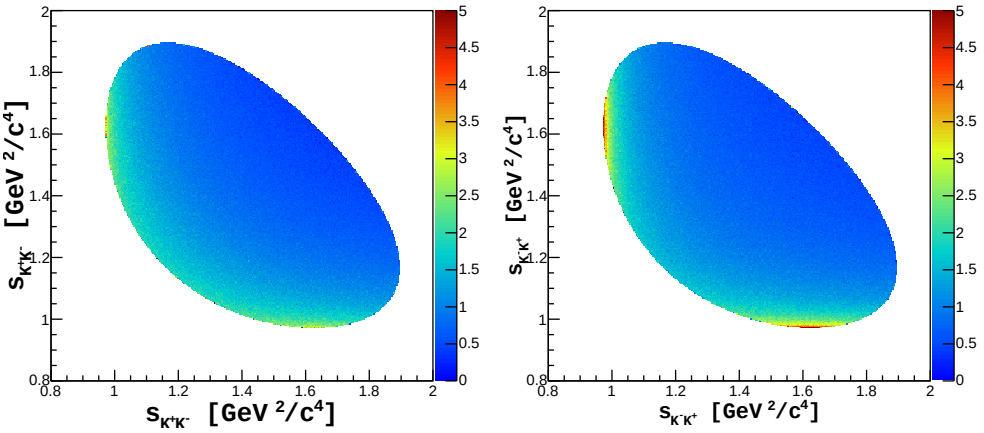

FIG. 11: Dalitz plot with the MC simulation of: the Flatté amplitude (left); the f_0 singlet component of the Triple-M (right).

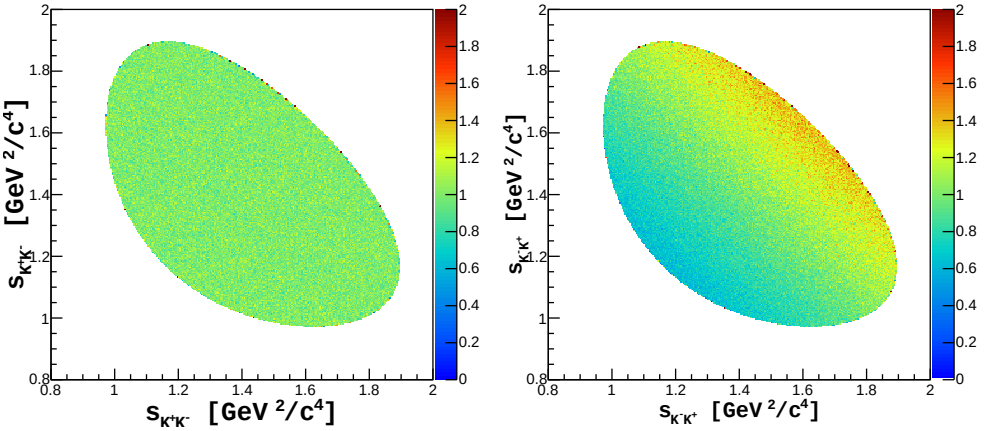

FIG. 12: Dalitz plot with the MC simulation of: an uniform nonresonant amplitude (left); the nonresonant component of the Triple-M (right).

between T_{NR} and the constant nonresonant amplitude, in Fig. 12, are much larger.

Finally, in Fig. 13, we present the Dalitz plot distribution with the full Triple-M amplitude as proposed in section V. One interesting feature is the distribution of events in the ϕ region. One of the lobes is depleted with respect to the other, resulting in a peak and a dip. This is caused by the interference between the ϕ and the f_0 components of the Triple-M amplitude. In this region the strong phases are rapidly changing. The resulting distribution of events is very sensitive to the details of the parametrization of these two components.

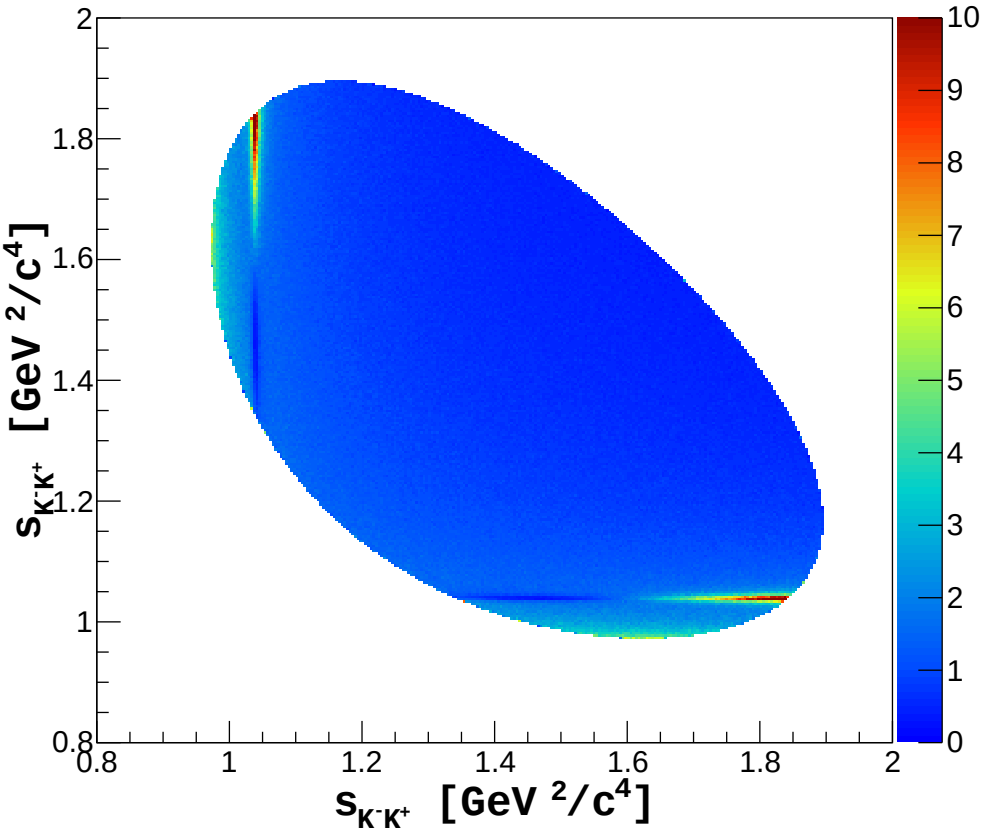

FIG. 13: Dalitz plot with MC simulation of the full Triple-M amplitude. The is assumed to be a singlet state. The hypothesis of the f_0 being an octet state yields a nearly identical distribution.

VII. CONCLUSIONS

In this paper, a new approach to decay amplitudes for non-leptonic three-body decays is presented, applied to the particular case $D^+ \to K^-K^+K^+$. Results, however, can be easily extended to other decays of charged heavy mesons into final states containing three charged kaons. This amplitude relies on matrix elements of weak currents involving multi-meson topologies and is called multi-meson-model, Triple-M, for short. The topologies considered are a direct consequence of chiral perturbation theory [12–14] and relevant to decays of both leptons and heavy mesons. These structures generalize the notion of form factor and, at the same time, allow one to go beyond the isobar model, often employed in analyses of heavy-meson decays.

We assume that the decay $D^+ \to K^-K^+K^+$ is dominated by the direct annihilation

$D^+ \to W^+$ which, subsequently gives rise to the processes shown in Fig. 3. The corresponding amplitude is proportional to the product of matrix elements $\langle (KKK)^+|A^\mu|0\rangle\langle 0|A_\mu|M^+\rangle$, where A^μ is the axial current. The Triple-M is composed by a non-resonant term and two resonant contributions, associated with the ϕ and the f_0. The non-resonant amplitude is a direct prediction from chiral symmetry and represented by a polynomial, with no free parameters. It describes a proper three-body interaction, rather than the of 2+1 decomposition (two-body subsystem+spectator). As this contribution involves no loops, it is real for theoretical reasons and, therefore, adequate for fixing the overall phase of the Triple-M amplitude.

The resonant contributions involve expressions which are very different from the A_k used in the isobar model amplitude $A = \sum c_k\, A_k$, but these expressions yield a similar line shape. However, in the Triple-M, the free coefficients c_k are absent, because the intensity of each resonance is predicted by the underlying dynamics. In particular, the ϕ contribution is completely fixed, for its intensity is related directly with the decay width into $\bar{K}K$. The case of the f_0 is different, just because one does not have precise values for its mass and couplings. Therefore, the three parameters in the amplitude, namely m_{f_0}, c_d, and c_m, are left to be determined by fits to data. In the $K^-K^+K^+$ final state one can access only the tail of the f_0, and therefore this channel may not be the best one for the determination of these three parameters. The decay $D_s^+ \to \pi^-\pi^+\pi^+$, where the $f_0(980)$ is the dominant component, would be the most adequate for this measurement. It is worth mentioning a recent work [21] on this subject, where the $f_0(980)$ line shape is obtained in the context of the Chiral Unitary theory, from a study of D_s^+ decays into $\pi^-\pi^+\pi^+$ and $K^-K^+K^+$.

Our study also encompasses other dynamical effects, representing corrections to the intermediate $\bar{K}K$ scattering amplitude, which were discussed in section IV and found to be small. We have left them out of the Triple-M, for the time being, since the ability of the leading contributions to reproduce data must be tested first. This kind of testing would provide important indications about the importance of effects which are not included in the the present version of the Triple-M, such as isospin 1 resonances, as well as dynamical effects associated with processes other than the annihilation diagram.

ACKNOWLEDGMENTS

This work was supported by Conselho Nacional de Desenvolvimento Científico e Tecnológico (CNPq) and M.R.R. would like to thank Fundação de Amparo à Pesquisa do Estado de São Paulo (FAPESP).

Appendix A: two-meson propagator

The results presented here are conventional and displayed for the sake of completeness. One deals with both S- and P-waves and the corresponding two-meson propagators are associated with the integrals

$$I_{aa} = \int \frac{d^4\ell}{(2\pi)^4} \frac{1}{D_-\ D_+}, \tag{A1}$$

$$I^{\mu\nu}_{aa} = \int \frac{d^4\ell}{(2\pi)^4} \frac{\ell^\mu \ell^\nu}{D_-\ D_+}, \tag{A2}$$

$$D_\pm = (\ell - q/2)^2 \pm M_a^2\ ,$$

with $q^2 = s$. The integral I_{aa} can be evaluated using dimensional techniques [13] and reads [22]

$$I_{aa} = -\frac{i}{16\pi^2}\left[R + \ln\frac{M_a^2}{\mu^2} + 1\right] - i\,\bar{\Omega}^S_{aa}\ , \tag{A3}$$

where R is a function of the number of dimensions n, which diverges in the limit $n \to 4$[22], μ is the renormalization scale, and $\bar{\Omega}^S_{aa}$ the regular part which, for $s \geq 4M_a^2$, has the form

$$\bar{\Omega}^S_{aa} = -\frac{1}{16\pi^2}\left\{2 - \sqrt{\frac{s-4M_a^2}{s}}\ln\left[\frac{s - 2M_a^2 + \sqrt{s(s-4M_a^2)}}{2M_a^2}\right] + i\,\pi\sqrt{\frac{s-4M_a^2}{s}}\right\}. \tag{A4}$$

In the renormalization process, the divergent factor R is replaced by an undetermined constant. However, there is no need to face this problem here, since we are concerned just with on-shell contributions to the propagator, associated with its imaginary part. Thus,

$$\bar{\Omega}^S_{aa} \to -i\,\frac{1}{16\pi}\,\frac{\sqrt{s-4M_a^2}}{\sqrt{s}} \tag{A5}$$

The integral $I^{\mu\nu}_{aa}$ is evaluated by noting that its Lorentz structure yields

$$I^{\mu\nu}_{aa} = g^{\mu\nu}\,A + q^\mu q^\nu\,B\ , \tag{A6}$$

where A and B are functions of s. Multiplying both eqs.(A2) and (A6), successively by $2q_\mu$ and by $g_{\mu\nu}$, using $2q\cdot\ell = D_+ - D_-$, $\ell^2 = -\,(s/4 - M_a^2) + (D_+ + D_-)/2$, and equating results, one finds the conditions

$$A + sB = I_a/2 \ ,$$

$$4A + sB = -(s/4 - M_a^2)\, I_{aa} + I_a \ ,$$

with

$$I_a = \int \frac{d^4\ell}{(2\pi)^4} \frac{1}{\ell^2 - M_a^2} = -i\, \frac{M_a^2}{16\pi^2} \left[R + \ln \frac{M_a^2}{\mu^2} \right] \ , \tag{A7}$$

which yield

$$I_{aa}^{\mu\nu} = \left[g^{\mu\nu} - \frac{q^\mu q^\nu}{q^2} \right] \left[-\frac{1}{4} \left(q^2 - 4M_a^2 \right) \ \frac{I_{aa}}{3} + \frac{I_a}{6} \right] + \frac{q^\mu q^\nu}{q^2} \ \frac{I_a}{2} \ . \tag{A8}$$

Keeping just the imaginary part, one has

$$I_{aa}^{\mu\nu} \to \frac{i}{4} \left[g^{\mu\nu} - \frac{q^\mu q^\nu}{s} \right] \ \bar{\Omega}_{aa}^P \ ,$$

$$\bar{\Omega}_{aa}^P \to -\frac{i}{48\pi} \frac{[s - 4\, M_a^2]^{3/2}}{\sqrt{s}} \ . \tag{A9}$$

Appendix B: partially dressed ϕ propagator

The bare ϕ propagator, $G_{\alpha\beta\gamma\delta}$, is given by eq.(A.10) of Ref. [14]. It is dressed by $\pi\rho$ and $\bar{K}K$ intermediate states and the corresponding self-energies are denoted respectively by $\Sigma_{\pi\rho}$ and $\Sigma_{\bar{K}K}$. In this appendix we consider just contributions of the first kind. The full propagator is given by

$$i\, \Delta_{\alpha\beta\gamma\delta} = i\, \Delta^{(0)}_{\alpha\beta\gamma\delta} + i\, \Delta^{(1)}_{\alpha\beta\gamma\delta} + i\, \Delta^{(2)}_{\alpha\beta\gamma\delta} + i\, \Delta^{(3)}_{\alpha\beta\gamma\delta} + \cdots \tag{B1}$$

$$i\, \Delta^{(0)}_{\alpha\beta\gamma\delta} = G_{\alpha\beta\gamma\delta} \tag{B2}$$

$$i\, \Delta^{(1)}_{\alpha\beta\gamma\delta} = G_{\alpha\beta ab} \ \left[-i\, \Sigma^{abcd} \right] \ G_{cd\gamma\delta} \tag{B3}$$

$$i\, \Delta^{(2)}_{\alpha\beta\gamma\delta} = G_{\alpha\beta ab} \ \left[-i\, \Sigma^{abef} \right] \ G_{efgh} \ \left[-i\, \Sigma^{ghcd} \right] \ G_{cd\gamma\delta} \tag{B4}$$

The $\phi\pi\rho$ interaction is extracted from the Lagrangian

$$\mathcal{L}^{\omega_1} = i\, g_1\, \epsilon^{\mu\nu\rho\sigma}\ \partial^\lambda \omega_{1\,\lambda\mu} \ \left[\partial_\nu \pi^- \rho^+_{\rho\sigma} + \partial_\nu \pi^+ \rho^-_{\rho\sigma} + \partial_\nu \pi^0 \rho^0_{\rho\sigma} \right] \tag{B5}$$

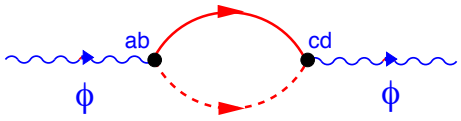

FIG. 14: Intermediate $\pi\rho$ contribution to the ϕ self-energy.

where $\omega_1 = \cos\theta\,\phi - \sin\theta\,\omega$ is the $SU(3)$ singlet component. In the sequence, we write $g_\epsilon = g_1\,\cos\theta$.

The self energy is given by

$$-i\,\Sigma^{abcd}_{\rho\pi} = \frac{(k^a\,g^{b\mu} - g^{a\mu}\,k^b)}{2}\;[H_{\mu\lambda}]\;\frac{(k^c\,g^{d\lambda} - g^{c\lambda}\,k^d)}{2}\;, \tag{B6}$$

$$H_{\mu\lambda} = \left[-3\,g_\epsilon^2\;I_{\mu\lambda}\right]\;, \tag{B7}$$

$$I_{\mu\lambda} = \frac{1}{i}\int\frac{d^4\ell}{(2\pi)^4}\,\frac{p^\mu\,p^\lambda}{p^2 - M_\pi^2}\,\epsilon_{\mu\nu\chi\eta}\,G_{\chi\eta\omega\zeta}(q)\,\epsilon_{\lambda\xi\omega\zeta}\;, \tag{B8}$$

with $p = k/2 - \ell$, $\quad q = k/2 + \ell$ and $k^2 = s$. Using the explicit form of $G_{\chi\eta\omega\zeta}$ and the definitions $D_\pi = p^2 - M_\pi^2$, $\;D_\rho = q^2 - m_\rho^2$, we find

$$I_{\mu\lambda} \to \frac{4}{m_\rho^2}\int\frac{d^4\ell}{(2\pi)^4}\,\frac{1}{D_\pi}\,\frac{1}{D_\rho} \tag{B9}$$
$$\times\left\{g_{\mu\lambda}\left[-m_\rho^2\left(M_\pi^2 + D_\pi\right) + \frac{1}{4}\,\left(s - M_\pi^2 - m_\rho^2 - D_\pi - D_\rho\right)^2\right] + \ell_\mu\ell_\lambda\left[k^2 - D_\rho\right]\right\}\;,$$

where we have used the fact that terms proportional to k_μ and k_λ do not contribute to eq.(B6). This integral is highly divergent, but the part regarding the $\pi\rho$ cut is not. Terms containing factors D_π and D_ρ in the numerator do not contribute to the cut function and the relevant integral is

$$I_{\mu\lambda} \to \frac{1}{m_\rho^2}\int\frac{d^4\ell}{(2\pi)^4}\,\frac{1}{D_\pi\,D_\rho}\left\{\left[s^2 - 2\,s\,\left(M_\pi^2 + m_\rho^2\right) + \left(M_\pi^2 - m_\rho^2\right)^2\right]g_{\mu\lambda} + 4\,s\,\ell_\mu\ell_\lambda\right\}\;. \tag{B10}$$

Using the definition

$$I_{\pi\rho} = \int\frac{d^4\ell}{(2\pi)^4}\,\frac{1}{D_\pi\,D_\rho} \tag{B11}$$

and the result

$$\int\frac{d^4\ell}{(2\pi)^4}\,\frac{\ell_\mu\,\ell_\lambda}{D_\pi\,D_\rho} = -\left\{\frac{1}{12\,k^2}\,\left[s^2 - 2\,s\,(M_\pi^2 + m_\rho^2) + (M_\pi^2 - m_\rho^2)^2\right]\,I_{\pi\rho}\right\}g_{\mu\lambda}$$
$$+\ \text{term proportional to}\,k_\mu\,k_\lambda\;, \tag{B12}$$

the relevant component of $I_{\mu\lambda}$ becomes

$$I_{\mu\lambda} \to \left\{ \frac{2}{3\,m_\rho^2}\ \left[s^2 - 2\,s\,(M_\pi^2 + m_\rho^2) + (M_\pi^2 - m_\rho^2)^2\right]\ I_{\pi\rho} \right\}\ g_{\mu\lambda}\ . \tag{B13}$$

The on-shell contribution to eq.(B11) is given by

$$I_{\pi\rho} = -\ \frac{1}{16\,\pi}\frac{\sqrt{\lambda_{\pi\rho}}}{s}\ , \tag{B14}$$

with $\lambda_{\pi\rho} = \left[s^2 - 2\,s\,(M_\pi^2 + m_\rho^2) + (M_\pi^2 - m_\rho^2)^2\right] = 4\,s\,Q_{\pi\rho}^2$, where $Q_{\pi\rho}$ is the CM three-momentum. We then have

$$H_{\mu\lambda} = g_{\mu\lambda}\,\frac{m_\phi}{s}\ \Gamma_\phi^{\pi\rho}(s)\ , \tag{B15}$$

$$m_\phi\,\Gamma_\phi^{\pi\rho}(s) = \frac{g_\epsilon^2}{\pi\,m_\rho^2}\ s^{3/2}\,Q_{\pi\rho}^3\ . \tag{B16}$$

Using this result into eq.(B1) and ressumming the series, we get the partially dressed propagator

$$\begin{aligned} i\,\Delta_{\alpha\beta\gamma\delta}^{\pi\rho} &= G_{\alpha\beta\gamma\delta} \\ &+ \left[\frac{i\,m_\phi\,\Gamma_\phi^{\pi\rho}(s)/s}{D_\phi^{\pi\rho}(s)}\right]\frac{1}{2}\left[g_\alpha^d\,k_\beta\,k^c + g_\beta^c\,k_\alpha\,k^d - g_\alpha^c\,k_\beta\,k^d - g_\beta^d\,k_\alpha\,k^c\right]\ G_{cd\gamma\delta}\ , \end{aligned} \tag{B17}$$

where the denominator $D_\phi^{\pi\rho}(s)$ is given by

$$D_\phi^{\pi\rho} = s - m_\phi^2 + i\,m_\phi\,\Gamma_\phi^{\pi\rho}(s)\ . \tag{B18}$$

In the evaluation of amplitudes involving a $\bar{K}(p_1)\,K(p_2)$ vertex, one encounters the product

$$i\,\Delta_{\alpha\beta\gamma\delta}\ \left(p_1^\gamma p_2^\delta - p_2^\gamma p_1^\delta\right) = -\ \frac{2\,i}{D_\phi^{\pi\rho}(s)}\ \left[p_{1\alpha}p_{2\beta} - p_{2\alpha}p_{1\beta}\right]\ . \tag{B19}$$

Appendix C: $\bar{K}K$ amplitude

We construct the $\bar{K}K$ amplitude by deriving interaction kernels $\mathcal{K}$ from chiral Lagrangians [14] involving resonances and iterating them in the s-channel, by means of two-kaon loops. In the treatment of the S-channel, one considers the coupling of $\pi\pi$ and $\bar{K}K$ states, whereas in the P-channel we distinguish K^-K^+ and $\bar{K}^0K^0$ intermediate states.

1. coupled channel formalism

Basic formulae given here apply to both S- and P- channels. In the absence of coupling, the amplitudes t are given as sums of Dyson series

$$t_{11} = \frac{\mathcal{K}_{11}}{1 + \Omega_{11}\,\mathcal{K}_{11}} \,, \tag{C1}$$

$$t_{22} = \frac{\mathcal{K}_{22}}{1 + \Omega_{22}\,\mathcal{K}_{22}} \tag{C2}$$

where the functions Ω_{ii} describe the propagation of two intermediate meson of mass M_i.

In the diagonal channels, one can construct effective kernels $\bar{\mathcal{K}}$, given by

$$\bar{\mathcal{K}}_{11} = \mathcal{K}_{11} - \mathcal{K}_{12}\,\left[1 - \Omega_{22}\,t_{22}\right]\,\Omega_{22}\,\mathcal{K}_{21} \,, \tag{C3}$$

$$\bar{\mathcal{K}}_{22} = \mathcal{K}_{22} - \mathcal{K}_{21}\,\left[1 - \Omega_{11}\,t_{11}\right]\,\Omega_{11}\,\mathcal{K}_{12} \,, \tag{C4}$$

The diagonal coupled amplitudes T are obtained by iterating the effective kernels and read

$$T_{11} = \frac{\bar{\mathcal{K}}_{11}}{1 + \Omega_{11}\,\bar{\mathcal{K}}_{11}} \,, \tag{C5}$$

$$T_{22} = \frac{\bar{\mathcal{K}}_{22}}{1 + \Omega_{22}\,\bar{\mathcal{K}}_{22}} \,, \tag{C6}$$

and their explicit forms are

$$T_{11} = \frac{\mathcal{K}_{11} + \Omega_{22}\,||\mathcal{K}||}{1 + \Omega_{11}\,\mathcal{K}_{11} + \Omega_{22}\,\mathcal{K}_{22} + \Omega_{11}\,\Omega_{22}\,||\mathcal{K}||} \,, \tag{C7}$$

$$T_{22} = \frac{\mathcal{K}_{22} + \Omega_{11}\,||\mathcal{K}||}{1 + \Omega_{11}\,\mathcal{K}_{11} + \Omega_{22}\,\mathcal{K}_{22} + \Omega_{11}\,\Omega_{22}\,||\mathcal{K}||} \,, \tag{C8}$$

with

$$||\mathcal{K}|| = \mathcal{K}_{11}\,\mathcal{K}_{22} - \mathcal{K}_{12}^2 \,. \tag{C9}$$

The off-diagonal term is

$$T_{12} = \frac{\mathcal{K}_{12}}{1 + \Omega_{11}\,\mathcal{K}_{11} + \Omega_{22}\,\mathcal{K}_{22} + \Omega_{11}\,\Omega_{22}\,||\mathcal{K}||} \,. \tag{C10}$$

2. S-channel amplitude

In the treatment of the S-channel, one needs three basic kernels, namely
$\mathcal{K}_{11} \to [\pi\pi \leftrightarrow \pi\pi]$, $\mathcal{K}_{12} \to [\pi\pi \leftrightarrow KK]$, $\mathcal{K}_{22} \to [KK \leftrightarrow KK]$.

As the role of the f_0 in the $SU(3)$ structure is not clear, we allow it to be either a singlet, with mass m_0, or a member of an octet, with mass m_8.

The relevant kernels read

$$\mathcal{K}_{11} = \frac{1}{F_\pi^2}\left[\frac{2s - M_\pi^2}{3} - \frac{4}{3}\,\frac{G_\pi^2}{s - m_0^2} - \frac{2}{3}\,\frac{G_\pi^2}{s - m_8^2}\,,\right] \tag{C11}$$

$$\mathcal{K}_{22} = \frac{1}{F_K^2}\left[\frac{3\,s}{8} - \frac{4}{3}\,\frac{G_K^2}{s - m_0^2} - \frac{1}{6}\,\frac{G_K^2}{s - m_8^2}\right]\,, \tag{C12}$$

$$\mathcal{K}_{12} = \frac{1}{F_\pi F_K}\left[\frac{s}{4} - \frac{4}{3}\,\frac{G_\pi\,G_K}{s - m_0^2} + \frac{1}{3}\,\frac{G_\pi\,G_K}{s - m_8^2}\right]\,, \tag{C13}$$

with

$$G_\pi = \frac{1}{F_\pi}\left[c_d\,s - 2\,(c_d - c_m)\,M_\pi^2\right]\,, \tag{C14}$$

$$G_K = \frac{1}{F_K}\left[c_d\,s - 2\,(c_d - c_m)\,M_K^2\right]\,, \tag{C15}$$

where c_d and c_m are coupling constants [14] and we have used $\tilde{c}_i = c_i/\sqrt{3}$.

In the K-matrix approximation, one needs just the on-shell component of the two-meson propagators, which are given by

$$\Omega_{\pi\pi} = -\left[\frac{3}{2}\right]\,\frac{i}{16\,\pi}\,\frac{\sqrt{s - 4\,M_\pi^2}}{\sqrt{s}} = -\,\frac{3i}{16\,\pi}\,\frac{Q_{\pi\pi}}{\sqrt{s}}\,, \tag{C16}$$

$$\Omega_{KK} = -\left[\frac{4}{2}\right]\,\frac{i}{16\,\pi}\,\frac{\sqrt{s - 4\,M_K^2}}{\sqrt{s}} = -\,\frac{i}{4\,\pi}\,\frac{Q_{KK}}{\sqrt{s}}\,, \tag{C17}$$

which include both the multiplicities of intermediate states and the symmetry factor 1/2.

The scattering amplitudes can be obtained by using eqs.(C11-C17) into results (C7-C10). However, this yields expressions which are rather cumbersome. In order to simplify the results, we neglect contact interactions in eqs.(C11-C13) and assume the $f_0(980)$ to be either a $SU(3)$ singlet or a member of an octed. These choices are indicated, respectively, by labels 0 and 8.

In the singlet case, one has

$$T_{11}^0 = -\frac{4\,G_\pi^2}{3F_\pi^2}\,\frac{1}{D_0}\,, \qquad T_{22}^0 = -\frac{4\,G_K^2}{3F_K^2}\,\frac{1}{D_0}\,, \qquad T_{12}^0 = -\frac{4\,G_\pi\,G_K}{3F_\pi F_K}\,\frac{1}{D_0}\,, \tag{C18}$$

$$D_0 = \left(s - m_{f_0}^2\right) + i\, m_{f_0}\, \Gamma_0 \ , \tag{C19}$$

$$m_{f_0}\, \Gamma_0 = \frac{G_\pi^2}{4\pi F_\pi^2}\, \frac{Q_{\pi\pi}}{\sqrt{s}} + \frac{G_K^2}{3\pi F_K^2}\, \frac{Q_{KK}}{\sqrt{s}} \ . \tag{C20}$$

Alternatively, for the octet, one finds

$$T_{11}^8 = -\frac{2\, G_\pi^2}{3F_\pi^2}\, \frac{1}{D_8} \ , \qquad T_{22}^8 = -\frac{G_K^2}{6F_K^2}\, \frac{1}{D_8} \ , \qquad T_{12}^8 = \frac{G_\pi\, G_K}{3F_\pi F_K}\, \frac{1}{D_8} \ , \tag{C21}$$

$$D_8 = \left(s - m_{f_0}^2\right) + i\, m_{f_0}\, \Gamma_8 \ , \tag{C22}$$

$$m_{f_0}\, \Gamma_8 = \frac{G_\pi^2}{8\pi F_\pi^2}\, \frac{Q_{\pi\pi}}{\sqrt{s}} + \frac{G_K^2}{24\pi F_K^2}\, \frac{Q_{KK}}{\sqrt{s}} \ . \tag{C23}$$

3. P-channel amplitude

In the P-channel, we consider the kernels
$\mathcal{K}_{11} \to [K^-K^+ \leftrightarrow K^-K^+]$, $\mathcal{K}_{12} \to [\bar{K}^0K^0 \leftrightarrow \bar{K}^0K^0]$, $\mathcal{K}_{22} \to [K^-K^+ \leftrightarrow \bar{K}^0K^0]$.

They are related to tree amplitude is given by $(t-u)\,\mathcal{K}$ and given by

$$\mathcal{K}_{11} = \mathcal{K}_{22} = -\mathcal{K}_{12} = \mathcal{K}_0^P/2 \ , \tag{C24}$$

with

$$\mathcal{K}_0^P(s) = \frac{3}{4\, F_K^2} - \left[\sin^2\theta\, \frac{3\, G_V^2}{2\, F_K^4}\right]\, \frac{s}{D_\phi^{\pi\rho}(s)} \ . \tag{C25}$$

In the evaluation of amplitudes, it is convenient to express it as

$$\mathcal{K}_0^P(s) = \frac{N_0^P(s)}{D_\phi^{\pi\rho}(s)} \ , \tag{C26}$$

$$N_0^P(s) = -\left\{\sin^2\theta\, \frac{3\, G_V^2}{2\, F_K^4}\, s - \frac{3\, D_\phi^{\pi\rho}}{4\, F_K^2}\right\} \ , \tag{C27}$$

The two-kaon propagators are

$$\Omega_{11}^P = -\frac{i}{48\,\pi}\, \frac{[s - 4\, M_{K^+}^2]^{3/2}}{\sqrt{s}} = -\frac{i}{6\,\pi}\, \frac{|Q_{11}|^3}{\sqrt{s}} \ , \tag{C28}$$

$$\Omega_{22}^P = -\frac{i}{48\,\pi}\, \frac{[s - 4\, M_{K^0}^2]^{3/2}}{\sqrt{s}} = -\frac{i}{6\,\pi}\, \frac{|Q_{22}|^3}{\sqrt{s}} \ . \tag{C29}$$

These results yield the various components of the KK amplitude, which are given by

$$T_{11} = T_{22} = -T_{12} = T_0^P/2 \ . \tag{C30}$$

Its explicit form is

$$T_0^P(s) = \frac{\mathcal{K}_0^P}{1 + [\Omega_{11}^P + \Omega_{22}^P]\,\mathcal{K}_0^P} = \frac{N_0^P(s)}{D_\phi(s)} \tag{C31}$$

$$D_\phi(s) = s - m_\phi^2 + i\, m_\phi\, \Gamma_\phi(s) - i\, \frac{1}{6\pi}\, \frac{3}{4F_K^2}\, \frac{D_\phi^{\pi\rho}(s)}{\sqrt{s}}\, \left(Q_{11}^3 + Q_{22}^3\right)$$

$$m_\phi\, \Gamma_\phi(s) = \left[\frac{1}{6\pi}\, \sin^2\theta\, \frac{3\, G_V^2}{2\, F_K^4}\, \sqrt{s}\, \left(Q_{11}^3 + Q_{22}^3\right) + \frac{1}{\pi}\, \frac{g_\epsilon^2}{m_\rho^2}\, s^{3/2}\, Q_{\pi\rho}^3\right] \tag{C32}$$

For $s = m_\phi^2$, the imaginary part of D_ϕ becomes equal to $m_\phi\, \Gamma_\phi$. Using $\Gamma_\phi = \Gamma_{\pi\rho} + \Gamma_{KK}$, we determine the coupling constants, which are given by

$$\frac{\sin^2\theta}{6\,\pi}\, \frac{3\, G_V^2}{2\, F_K^4} = \frac{\Gamma_{KK}}{(\tilde{Q}_{11}^3 + \tilde{Q}_{22}^3)}\,, \tag{C33}$$

$$\frac{1}{\pi}\, \frac{g_\epsilon^2}{m_\rho^2} = \frac{\Gamma_{\pi\rho}}{m_\phi^2\, \tilde{Q}_{\pi\rho}^3}\,, \tag{C34}$$

where $\tilde{Q} \equiv Q(s = m_\phi^2)$. These results allow eqs.(C27) and (C32) to be written as

$$N_0^P = -\frac{6\pi\, \Gamma_{KK}}{(\tilde{Q}_{cc}^3 + \tilde{Q}_{nn}^3)}\, s + \frac{3\, D_\phi^{\pi\rho}}{4\, F_K^2}\,, \tag{C35}$$

$$D_\phi^{\pi\rho} = s - m_\phi^2 + i\, \Gamma_{\pi\rho}\, \frac{s^{3/2}}{m_\phi^2}\, \frac{Q_{\pi\rho}^3}{\tilde{Q}_{\pi\rho}^3}\,, \tag{C36}$$

$$m_\phi\, \Gamma_\phi(s) = \left[\Gamma_{KK}\, \sqrt{s}\, \frac{(Q_{11}^3 + Q_{22}^3)}{(\tilde{Q}_{11}^3 + \tilde{Q}_{22}^3)} + \Gamma_{\pi\rho}\, \frac{s^{3/2}}{m_\phi^2}\, \frac{Q_{\pi\rho}^3}{\tilde{Q}_{\pi\rho}^3}\right]\,. \tag{C37}$$

Appendix D: production amplitudes

1. *S*-channel

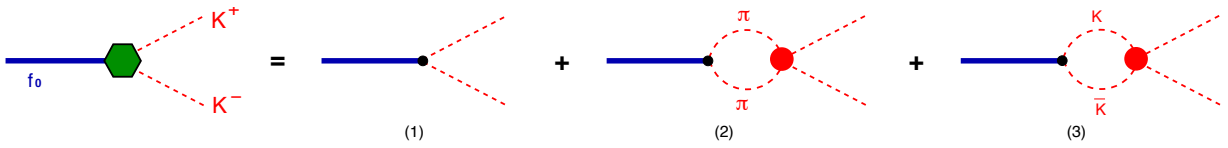

FIG. 15: f_0 production with $K\bar{K}$ and $\pi\pi$ couple channel contribution.

The production amplitude for a final charged K^-K^+ pair in the S-channel is defined in Fig. 15 and includes $\pi\pi$ and $\bar{K}K$ loops coupled to the $f_0(980)$.

In the case of a singlet f_0, the diagrams above are described by

$$i\,\Pi^0_{(1)} + i\,\Pi^0_{(2)} + i\,\Pi^0_{(3)} = -\,\frac{2\,G_K}{\sqrt{3}\,F_K}\,\frac{1}{s-m_0^2}\left[1+\frac{\Omega_{11}}{D_0}\,\frac{4\,G_\pi^2}{3\,F_\pi^2}\,+\frac{\Omega_{22}}{D_0}\,\frac{4\,G_K^2}{3\,F_K^2}\right]$$

$$= i\,\Pi^0 = -\,\frac{2\,G_K}{\sqrt{3}\,F_K}\,\frac{1}{D_0}\,, \tag{D1}$$

with D_0 given by eq.(C19).

If the f_0 is as a member of an octet, we get

$$i\,\Pi^8_{(1)} + i\,\Pi^8_{(2)} + i\,\Pi^8_{(3)} = \frac{G_K}{\sqrt{6}\,F_K}\,\frac{1}{s-m_8^2}\left[1+\frac{\Omega_{11}}{D_8}\,\frac{2\,G_\pi^2}{3\,F_\pi^2}\,+\frac{\Omega_{22}}{D_8}\,\frac{G_K^2}{6\,F_K^2}\right]$$

$$= i\,\Pi^8 = \frac{G_K}{\sqrt{6}\,F_K}\,\frac{1}{D_8}\,, \tag{D2}$$

with D_8 as in eq.(C22).

2. P-channel

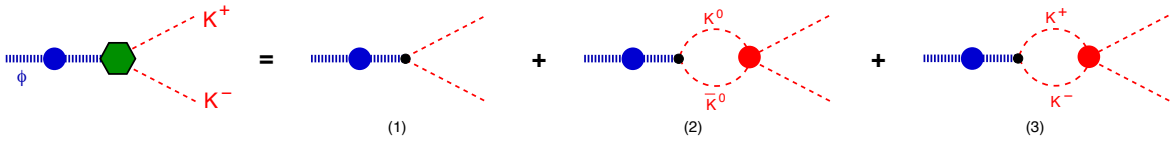

FIG. 16: ϕ production with propagator dressed by $\pi\rho$ and, K^+K^- and $K_0\bar{K}_0$ couple channel contribution.

The production amplitude $\Pi_{\alpha\beta\gamma\delta}$ is defined by the processes indicated in Fig. 16. Explicit evaluation yields

$$i\,\Pi_{(1)\,\alpha\beta} + i\,\Pi_{(2)\,\alpha\beta} + i\,\Pi_{(3)\,\alpha\beta}$$

$$= 2\,i\,\left[\sin\theta\,\frac{\sqrt{3}\,G_V}{2F_K^2}\right]\,\frac{1}{D_\phi^{\pi\rho}}\left[1-\Omega_{11}^P\,T_{11}^P-\Omega_{22}^P\,T_{22}^P\right]\left[p_{1\alpha}\,p_{2\beta}-p_{2\alpha}\,p_{1\beta}\right]$$

$$= i\,\Pi_{\alpha\beta} = 2\,i\,\left[\sin\theta\,\frac{\sqrt{3}\,G_V}{2F_K^2}\right]\,\frac{\left[p_{1\alpha}\,p_{2\beta}-p_{2\alpha}\,p_{1\beta}\right]}{D_\phi(s)}\,. \tag{D3}$$

Appendix E: individual tree currents

Individual contributions from the direct reading of the diagrams of Fig. 2 to the matrix element $A^\mu \equiv \langle K^-(p_1)K^+(p_2)K^+(p_3)|A^\mu|\,0\,\rangle$ are given below.

$$A^\mu_{(1)} = i\,\left[\frac{2\,\sqrt{2}}{3F_K}\right]\,(2\,p_1 - p_2 - 2\,p_3)^\mu\,, \tag{E1}$$

$$A^\mu_{(2)} = -i\,\left[\frac{2\sqrt{2}}{3F_K}\right]\,\frac{P^\mu}{P^2 - M_K^2}\,\left[p_1\cdot(p_2+p_3) - 2\,p_2\cdot p_3 + M_K^2\right]\,, \tag{E2}$$

$$A^\mu_{(3)} = -i\,\left[\sin^2\theta\,\frac{3\sqrt{2}\,F_V G_V}{2F_K^3}\right]\,\frac{[\,P\cdot p_2\,p_1^\mu - P\cdot p_1\,p_2^\mu\,]}{D_\phi^{\pi\rho}(m_{12}^2)}\,, \tag{E3}$$

$$A^\mu_{(4)} = i\,\left[\sin^2\theta\,\frac{3\sqrt{2}\,G_V^2}{F_K^3}\right]\,\frac{[\,p_2\cdot p_3\,p_1^\mu - p_1\cdot p_3\,p_2^\mu\,]}{D_\phi^{\pi\rho}(m_{12}^2)}\,, \tag{E4}$$

$$A^\mu_{(5)} = -i\,\left[\sin^2\theta\,\frac{3\sqrt{2}\,G_V^2}{F_K^3}\right]\,\frac{P^\mu}{P^2 - M_K^2}\,\frac{[\,P\cdot p_1\,p_2\cdot p_3 - P\cdot p_2\,p_1\cdot p_3\,]}{D_\phi^{\pi\rho}(m_{12}^2)}\,, \tag{E5}$$

$$A^\mu_{(6)} = i\,\left[\frac{2\,\gamma_n\,\sqrt{2}\,c_d}{3\;F_K^3}\right]\,p_3^\mu\,\frac{[c_d\,p_1\cdot p_2 + c_m\,M_K^2]}{m_{12}^2 - m_{f_0}^2}\,, \tag{E6}$$

$$A^\mu_{(7)} = -i\,\left[\frac{2\,\gamma_n\,\sqrt{2}}{3\;F_K^3}\right]\,\frac{P^\mu}{P^2 - M_K^2}\,\left[c_d\,P\cdot p_3 - c_m\,M_K^2\right]\,\frac{[c_d\,p_1\cdot p_2 + c_m\,M_K^2]}{m_{12}^2 - m_{f_0}^2}\,. \tag{E7}$$

---

[1] D. Asner, arXiv:hep-ex/0410014 (2004).

[2] L-L. Chau, Phys. Rep. **95**, 1 (1983).

[3] P. C. Magalhães, M. R. Robilotta, K. S. F. F. Guimarães, T. Frederico,W. S. de Paula, I. Bediaga, A. C. dos Reis, and C.M. Maekawa, Phys. Rev. D**84**, 094001 (2011).

[4] P.C. Magalhães and M.R. Robilotta, "$D^+ \to K^-\pi^+\pi^+$ - the weak vector current", Phys.Rev. **D92** 9, 094005 (2015) [arXiv:1504.06346].

[5] K.S.F.F. Guimarães, W. de Paula, I. Bediaga, A. Delfino, T. Frederico, A. C. dos Reis and L. Tomio, "Relativistic three-body model for final state interaction in $D \to K\pi\pi$ decay", Nucl. Phys. B (Proc. Suppl.) **199** (2010) 341.

[6] Franz Niecknig, and Bastian Kubis, Dispersion-theoretical analysis of the $D^+ \to K^-\pi^+\pi^+$ Dalitz plot, JHEP **10**, 142 (2015).

[7] S. X. Nakamura, arXiv:1504.02557 (2015).

[8] G. Ecker and R. Unterdorfer, Eur.Phys.JC**24**, 535 (2002), Nucl.Phys.Proc.Suppl. **121**, 175 (2003).

[9] Bauer, Stich and Wirbel, Z. Phys. C **34**, 103 (1987)].

[10] G. Burdman and J.F. Donoghue, Phys. Lett. B **280**, 287 (1992); M.B. Wise, Phys.Rev. D**45**, R2188 (1992).

[11] D. R. Boito, R. Escribano, Phys. Rev. D **80**, 054007 (2009); M. Diakonou and F. Diakonos, Phys. Lett. B **216**, 436 (1989).

[12] S. Weinberg, Physica A **96**, 327 (1979).

[13] J. Gasser and H. Leutwyler, Ann. Phys. **158**, 142 (1984); Nucl. Phys. B**250**, 465 (1985).

[14] G. Ecker, J. Gasser, A. Pich and E. De Rafael, Nucl. Phys. B **321**, 311 (1989).

[15] J.A. Oller and E. Oset, Phys. Rev. D **60**, 074023 (1999); Nucl. Phys. A **620**, 465 (1997); A **652**, 407(E) (1999).

[16] J.H. Kühn and E. Mirkes, Z. Phys. **C 56**, 661 (1992).

[17] K. Nakamura et al. (Particle Data Group), J. Phys. G 37, 075021 (2010).

[18] S.M. Flatté, Phys. Lett. B **63** , 224 (1976).

[19] M. Ablikim *et al.* , BES Collaboration, Phys. Lett B 607, 243 (2005).

[20] M. Jamin, J.A. Oller and A. Pich, Nucl. Phys. B **587**, 331 (2000).

[21] J. M. Dias, F. S. Navarra, M. Nielsen and E. Oset, arXiv:1601.04635 [hep-ph].

[22] S. Scherer, Adv. Nucl. Phys. **27**, 277 (2003).